Article

Probing the Kinetic Landscape of Transient Peptide–Protein Interactions by Use of Peptide ^{15}N NMR Relaxation Dispersion Spectroscopy: Binding of an Antithrombin Peptide to Human Prothrombin

Dmitri Tolkatchev, Ping Xu, and Feng Ni

J. Am. Chem. Soc., **2003**, 125 (41), 12432-12442• DOI: 10.1021/ja021238l • Publication Date (Web): 17 September 2003

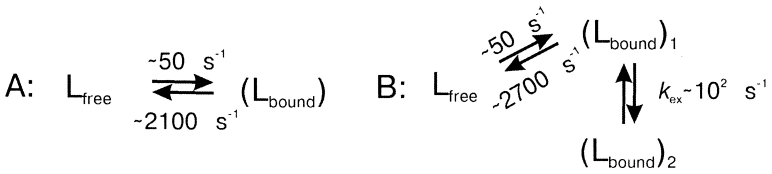

More About This Article

Additional resources and features associated with this article are available within the HTML version:

- Supporting Information
- Links to the 5 articles that cite this article, as of the time of this article download
- Access to high resolution figures
- Links to articles and content related to this article
- Copyright permission to reproduce figures and/or text from this article

View the Full Text HTML

J|A|C|S
ARTICLES
Published on Web 09/17/2003

Probing the Kinetic Landscape of Transient Peptide−Protein Interactions by Use of Peptide ^{15}N NMR Relaxation Dispersion Spectroscopy: Binding of an Antithrombin Peptide to Human Prothrombin

Dmitri Tolkatchev, Ping Xu, and Feng Ni*

Contribution from the Biomolecular NMR and Protein Research Laboratory, Biotechnology Research Institute, National Research Council of Canada, Montreal, Quebec, Canada H4P 2R2

Received October 3, 2002; Revised Manuscript Received July 24, 2003; E-mail: Feng.Ni@cnrc-nrc.gc.ca

Abstract: Protein−ligand interactions may lead to the formation of multiple molecular complexes in dynamic exchange, affecting the kinetic and thermodynamic characteristics of the binding equilibrium. We followed the dissociation kinetics of the transient and specific complex of an antithrombotic peptide *N*-acetyl-*Asp$_{55}$-*Phe-*Glu-*Glu-*Ile-Pro$_{60}$-Glu-Glu-Tyr-Leu-Gln$_{65}$ with human prothrombin by use of ^{15}N NMR relaxation dispersion spectroscopy of the peptide. Every one of the five ^{15}N-labeled adjacent residues of the peptide exhibited apparently different kinetic exchange and relaxation behaviors, which were especially evident at different concentrations of prothrombin. Binding-induced ^{15}N relaxation dispersion of residues Phe$_{56}$, Glu$_{57}$, Glu$_{58}$, and Ile$_{59}$ can be fitted phenomenologically to a two-site on-and-off exchange mechanism with physically feasible relaxation and kinetic parameters obtained for residues Phe$_{56}$, Glu$_{58}$, and Ile$_{59}$, independent of the prothrombin concentration. The apparent kinetic parameters of Glu$_{57}$ show some dependence on the concentration of prothrombin and the extracted transverse relaxation rate for Glu$_{57}$ in the bound state was severalfold higher than that expected for a protein−peptide complex with a size of ∼72 kDa. In addition, the equilibrium population of the bound peptide obtained for Glu$_{57}$ was inconsistent with those for Phe$_{56}$, Glu$_{58}$, and Ile$_{59}$ and with the prothrombin/peptide ratios used in the experiments. These discrepancies can be explained by the presence of two conformations for the peptide−protein complex exchanging at a rate of ∼100 s^{-1}. In all, our study shows that fast dissociation of protein−peptide complexes can be studied quantitatively using peptide ^{15}N NMR relaxation dispersion measurements without a precise knowledge of the peptide and protein concentrations. In addition, protein titration was found to improve the accuracy of quantitative analysis and may make it possible to determine the rate of conformational changes within the protein−peptide complex.

The molecular nature of protein−ligand associations is a subject of long-standing interest in chemistry, in biochemistry, and particularly in the interdisciplinary field of pharmaceutical drug discovery.[1,2] Structural investigations have portrayed, at atomic resolution, the specific molecular interactions in many protein−ligand complexes and especially those formed between enzymes and inhibitors/substrates and between proteins and peptide ligands.[3−5] Thermodynamic analyses of complex formation, such as equilibrium binding experiments and enzyme inhibition assays, have provided valuable information regarding the molecular/atomic forces that dictate the structural stability of protein−ligand complexes.[1,2] In general, however, it is still difficult if not impossible to correlate quantitatively the detailed structural information with the binding affinity of protein−ligand complexes.[1] In most cases, the difficulties may be related to the failure to account for subtle molecular motions in the exact dimensions of protein−ligand interactions captured by high-resolution molecular structures.[1,6,7] On top of all these, there is still limited understanding of the relationship between the kinetics of binding and the molecular structures of protein−ligand complexes.[8−10] There are therefore significant interests in better ways to probe the kinetic mechanisms of molecular interactions, particularly the dissociation of transient protein−ligand complexes.[8−10]

A number of techniques are already available for following the kinetics of protein−protein and protein−ligand interactions, such as surface plasmon resonance[8,11] and analysis of the progress curves of enzyme inhibition by specific ligands.[10,12] All these methodologies are limited to the characterization of

(1) Kuntz, I. D.; Chen, K.; Sharp, K. A.; Kollman, P. A. *Proc. Natl. Acad. Sci. U.S.A* **1999**, *96*, 9997−10002.
(2) Brooijmans, N.; Sharp, K. A.; Kuntz, I. D. *Proteins* **2002**, *48*, 645−653.
(3) Petsko, G. A.; Ringe, D. *Curr. Opin. Chem. Biol.* **2000**, *4*, 89−94.
(4) Sem, D. S.; Pellecchia, M. *Curr. Opin. Drug Discovery Dev.* **2001**, *4*, 479−492.
(5) Blundell, T. L.; Jhoti, H.; Abell, C. *Nat. Rev. Drug Discovery* **2002**, *1*, 45−54.
(6) Nienaber, V. L.; Mersinger, L. J.; Kettner, C. A. *Biochemistry* **1996**, *35*, 9690−9699.
(7) Carlson, H. A. *Curr. Opin. Chem. Biol.* **2002**, *6*, 447−452.
(8) Van Regenmortel, M. H. *Cell Mol. Life Sci.* **2001**, *58*, 794−800.
(9) Andersson, K.; Choulier, L.; Hamalainen, M. D.; Van Regenmortel, M. H.; Altschuh, D.; Malmqvist, M. *J. Mol. Recognit.* **2001**, *14*, 62−71.
(10) Day, Y. S.; Baird, C. L.; Rich, R. L.; Myszka, D. G. *Protein Sci.* **2002**, *11*, 1017−1025.
(11) Wilson, W. D. *Science* **2002**, *295*, 2103−2105.

 10.1021/ja021238l CCC: $25.00 Published 2003 by the Am. Chem. Soc.

tight-binding or slow-dissociating protein−ligand complexes with lifetimes longer than at least several seconds.[8,10] Another limitation is that they only provide a macroscopic description of binding kinetics, without details of the dynamic behavior of the interacting molecules at atomic resolution. In particular, very little quantitative information is available for the fast dissociation of transient protein−ligand complexes with lifetimes ranging from a few milliseconds to hundreds of microseconds. Short-lived or transient, but specific-binding, protein−ligand complexes can be a good starting point for the design of high-affinity inhibitors or effector molecules.[13,14] Fast dissociating ligands are often derived from naturally occurring protein−protein interfaces[15] or discovered by screening against molecular libraries.[13,16] Even without affinity "maturation", these specific-binding ligands can be converted into bivalent and polyvalent molecules with a potential increase in affinity and the lifetimes of the protein−ligand complexes.[15−22]

The kinetics of transient inhibitor binding to large enzymes and proteins have been studied previously utilizing mostly ^{19}F NMR relaxation[23−28] or line shape analysis[29] and proton NMR relaxation measurements.[30] More recent work in this area has included the characterization of multiple conformational states in small protein−peptide complexes[31,32] and in enzyme−substrate/inhibitor interactions.[33−37] It has been shown that in complex protein systems protein−ligand interactions may involve a dynamic equilibrium of an ensemble of protein−ligand complexes with related or distinctly different structural configurations. Even the formation of a well-structured molecular complex may follow a process of conformational selection out of the ensemble of different conformational states for the unbound species.[38] Indeed, recent studies have demonstrated that binding of small hydrophobic molecules inside a well-structured protein is permitted by the existence of a significant population of protein conformations in partially open or "excited" states.[39]

In this paper, we use the newly developed ^{15}N T_2 (CPMG) relaxation experiments, or ^{15}N NMR relaxation dispersion spectroscopy,[40−43] to quantitate the kinetics of a transient molecular complex formed between an ^{15}N-labeled antithrombotic peptide and human prothrombin,[44,45] a protein larger than 70 kDa. On one hand, the specific binding of antithrombin peptides to the latent zymogen, prothrombin,[44] has remained a subject of significant interest, since the peptide binding site on prothrombin is involved in substrate recognition by the prothrombinase macromolecular assembly.[46] There is also the fundamental question of the changes in structural and dynamic properties of protein functional surfaces accompanying protein activation, for example, the conversion of prothrombin to active thrombin in blood coagulation.[44,45] On the other hand, it is particularly attractive to follow the kinetic behavior of peptide binding to large proteins, whenever the latter are not normally or easily accessible to direct (NMR) observation. The challenge here lies in the difficulty or impossibility to observe the bound state of the peptide ligand due to the high molecular weight of the peptide−protein complex, so that conclusions may depend on the kinetic mechanism chosen to explain the experimental data. We found that peptide ^{15}N NMR relaxation dispersion measurements, especially when performed at different concentrations of the binding protein, can be used to quantitate the dissociation rates and bound populations of transient protein−peptide complexes and detect the existence of alternative binding modes of the bound peptide.

Materials and Methods

The peptide *N*-acetyl-Hir(55−65) was enriched selectively with ^{15}N isotopes at the backbone amides of five residues Asp_{55}, Phe_{56}, Glu_{57}, Glu_{58}, and Ile_{59} to produce the labeled peptide *N*-acetyl-$^{*}D_{55}{}^{*}F{}^{*}E{}^{*}E{}^{*}IP_{60}EEYLQ_{65}$ as described previously.[47] The purified peptide material was dissolved at ∼1.5 mM in an aqueous solution that was 50 mM in NaCl and 50 mM in sodium phosphate at pH 5.5. Carefully measured volume aliquots of human prothrombin at a stock concentration of ∼0.3 mM were added to the peptide solution to produce molar ratios of ∼1:45, ∼1:35, and ∼1:30 for the prothrombin and peptide concentrations, respectively.

Proton resonance assignment was achieved by using 2D NOESY-{^{1}H−^{15}N}-HSQC with an NOE mixing time of 250 ms and 2D TOCSY-{^{1}H−^{15}N}-HSQC with a TOCSY mixing time of 56.6 ms[48] recorded at 288 K and 500 MHz. Amino acid residues were identified

(12) Pargellis, C. A.; Morelock, M. M.; Graham, E. T.; Kinkade, P.; Pav, S.; Lubbe, K.; Lamarre, D.; Anderson, P. C. *Biochemistry* **1994**, *33*, 12527−12534.
(13) Wells, J. A. *Science* **1996**, *273*, 449−450.
(14) Shuker, S. B.; Hajduk, P. J.; Meadows, R. P.; Fesik, S. W. *Science* **1996**, *274*, 1531−1534.
(15) Song, J.; Ni, F. *Biochem. Cell Biol.* **1998**, *76*, 177−188.
(16) Mourez, M.; Kane, R. S.; Mogridge, J.; Metallo, S.; Deschatelets, P.; Sellman, B. R.; Whitesides, G. M.; Collier, R. J. *Nat. Biotechnol.* **2001**, *19*, 958−961.
(17) Mammen, M.; Choi, S.-K.; Whitesides, G. M. *Angew. Chem. Int. Ed.* **1998**, *37*, 2754−2794.
(18) Rao, J.; Lahiri, J.; Isaacs, L.; Weis, R. M.; Whitesides, G. M. *Science* **1998**, *280*, 708−711.
(19) Kramer, R. H.; Karpen, J. W. *Nature* **1998**, *395*, 710−713.
(20) Kitov, P. I.; Sadowska, J. M.; Mulvey, G.; Armstrong, G. D.; Ling, H.; Pannu, N. S.; Read, R. J.; Bundle, D. R. *Nature* **2000**, *403*, 669−672.
(21) Fan, E.; Zhang, Z.; Minke, W. E.; Hou, Z.; Verlinde, C. L. M. J.; Hol, W. G. J. *J. Am. Chem. Soc.* **2000**, *122*, 2663−2664.
(22) Kiessling, L. L.; Gestwicki, J. E.; Strong, L. E. *Curr. Opin. Chem. Biol.* **2000**, *4*, 696−703.
(23) Sykes, B. D. *J. Am. Chem. Soc.* **1969**, *91*, 949−955.
(24) Smallcombe, S. H.; Ault, B.; Richards, J. H. *J. Am. Chem. Soc.* **1972**, *94*, 4585−4590.
(25) Gerig, J. T.; Stock, A. D. *Org. Magn. Res.* **1975**, *7*, 249−255.
(26) Gerig, J. T.; Halley, B. A.; Ortiz, C. E. *J. Am. Chem. Soc.* **1977**, *99*, 6219−6226.
(27) Dubois, B. W.; Evers, A. S. *Biochemistry* **1992**, *31*, 7069−7076.
(28) Peng, J. W. *J. Magn Reson.* **2001**, *153*, 32−47.
(29) Jacobson, A. R.; Gerig, J. T. *J. Biomol. NMR* **1991**, *1*, 131−144.
(30) Davis, D. G.; Perlman, M. E.; London, R. E. *J. Magn Reson. B* **1994**, *104*, 266−275.
(31) Hensmann, M.; Booker, G. W.; Panayotou, G.; Boyd, J.; Linacre, J.; Waterfield, M.; Campbell, I. D. *Protein Sci.* **1994**, *3*, 1020−1030.
(32) Gunther, U.; Mittag, T.; Schaffhausen; B. *Biochemistry* **2002**, *41*, 11658−11669.
(33) Perlman, M. E.; Davis, D. G.; Koszalka, G. W.; Tuttle, J. V.; London, R. E. *Biochemistry* **1994**, *33*, 7547−7559.
(34) Curto, E. V.; Moseley, H. N.; Krishna, N. R. *J. Comput.-Aided Mol. Des.* **1996**, *10*, 361−371.
(35) Deng, H.; Zhadin, N.; Callender, R. *Biochemistry* **2001**, *40*, 3767−3773.
(36) Gulotta, M.; Deng, H.; Deng, H.; Dyer, R. B.; Callender, R. H. *Biochemistry* **2002**, *41*, 3353−3363.
(37) Hammes, G. G. *Biochemistry* **2002**, *41*, 8221−8228.
(38) Tsai, C. D.; Ma, B.; Kumar, S.; Wolfson, H.; Nussinov, R. *Crit Rev. Biochem. Mol. Biol.* **2001**, *36*, 399−433.
(39) Mulder, F. A.; Mittermaier, A.; Hon, B.; Dahlquist, F. W.; Kay, L. E. *Nat. Struct. Biol.* **2001**, *8*, 932−935.
(40) Loria, J. P.; Rance, M.; Palmer, A. G. *J. Am. Chem. Soc.* **1999**, *121*, 2331−2332.
(41) Millet, O.; Loria, J. P.; Kroenke, C. D.; Pons, M.; Palmer, A. G. *J. Am. Chem. Soc.* **2000**, *122*, 2867−2877.
(42) Mulder, F. A. A.; Skrynnikov, N. R.; Hon, B.; Dahlquist, F. W.; Kay, L. E. *J. Am. Chem. Soc.* **2001**, *123*, 967−975.
(43) Akke, M. *Curr. Opin. Struct. Biol.* **2002**, *12*, 642−647.
(44) Ni, F.; Ning, Q.; Jackson, C. M.; Fenton, J. W. *J. Biol. Chem.* **1993**, *268*, 16899−16902.
(45) Anderson, P. J.; Nesset, A.; Dharmawardana, K. R.; Bock, P. E. *J. Biol. Chem.* **2000**, *275*, 16428−16434.
(46) Anderson, P. J.; Nesset, A.; Dharmawardana, K. R.; Bock, P. E. *J. Biol. Chem.* **2000**, *275*, 16435−16442.
(47) Carpenter, K. A.; Ni, F. *J. Magn. Reson.* **1992**, *99*, 192−197.
(48) Cavanagh, J.; Fairbrother, W. J.; Palmer, A. G.; Skelton, N. J. In *Protein NMR Spectroscopy: Principles and Practice*; Academic Press: San Diego, 1995.

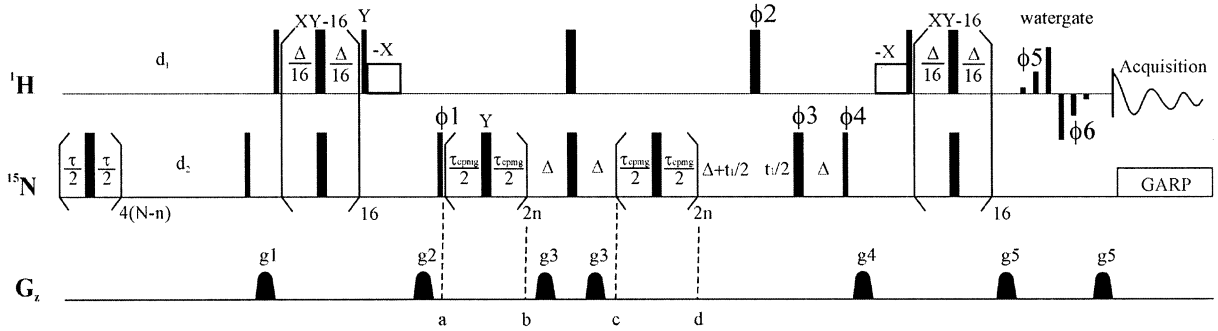

Figure 1. RF and field gradient pulse sequence for measuring the ^{15}N $R_2(1/\tau_{CPMG})$ dispersion profile with sensitivity enhancement and compensation of RF heating effects. A train of ^{15}N 180° pulses is applied at 100 ppm off the center of the HSQC spectrum with a separation of 1 ms at the beginning of the recycle delay d_1 such that the total number of ^{15}N 180° pulses, $4N$, is kept the same for all experiments with different CPMG pulse repetition rates. An XY-16 180° pulse train[50] is also applied to both the ^{1}H and ^{15}N nuclei during the two INEPT periods, which limits the decay of exchange-broadened ligand resonances. Further enhancement in sensitivity was achieved by using the 3919 WATERGATE sequence for water suppression.[51] The 90° and 180° RF pulses are represented by narrow and wide bars, respectively, applied along the $+X$ axis unless specified otherwise. The open rectangles are water-selective soft pulses with a duration of 2 ms. During data acquisition, ^{15}N decoupling is achieved using a GARP sequence[52] with an RF field of 1.0 kHz (at 500 MHz) or 1.2 kHz (at 800 MHz). The delays are $\Delta = 2.7$ ms, $\tau = 1$ ms, $d_2 = d_1 - 4(N - n)\tau$ and $\tau_{CPMG} = (T/4n - pw180_N)$, where T is the total duration of the ^{15}N CPMG pulse train and $pw180_N$ is the width of the ^{15}N 180° pulse. Sine bell-shaped gradient pulses with a duration of 1 ms are used with gradient strengths of $g_1 = 5G$/cm, $g_2 = -6G$/cm, $g_3 = 1.2G$/cm, $g_4 = 6G$/cm, and $g_5 = 10G$/cm. The phases of some RF pulses are the same as those reported previously with $\phi1 = +X\ -X$, $\phi2 = 4(+X)\ 4(-X)$, and $\phi3 = 2(+X)\ 2(+Y)\ 2(-X)\ 2(-Y)$,[41] except that the phases for the last ^{15}N 90° pulse, the WATERGATE sequence, and the RF receiver are cycled as $\phi4 = 4(+X)\ 4(-X)$, $\phi5 = 8(+X)\ 8(+Y)$, $\phi6 = 8(-X)\ 8(-Y)$ and receiver $= (+X\ -X\ -X\ +X)\ 2(-X\ +X\ +X\ -X)\ (+X\ -X\ -X\ +X)$. Phase-sensitive {^{1}H−^{15}N}-HSQC spectra were obtained by incrementing $\phi4$, according to the States−TPPI scheme.[53] The relaxation dispersion profile is derived from the spectral peak intensities at different effective B_1 fields,[54] expressed by the equation $R_2(1/\tau_{CPMG}) = -\ln[I(1/\tau_{CPMG})/I(0)]/T$,[42] where $I(1/\tau_{CPMG})$ is the intensity of an HSQC peak with varying n, hence the τ_{CPMG} delay, and $I(0)$ is the intensity of the same HSQC peak in the absence of the ^{15}N CPMG pulse trains (i.e., $n = 0$ in periods a and b and periods c and d). NMR data were collected at ^{15}N frequencies of 50.684 and 81.076 MHz using Bruker Avance/DRX 500 and 800 MHz NMR spectrometers. The total length of the ^{15}N CPMG pulse train, T, is kept at a constant value of 40 ms for all the experiments. The total number ($4N$) of the ^{15}N CPMG 180° pulses was set to 100.

on the basis of the cross-peak patterns from the TOCSY spectrum and assigned through sequential NOE connectivities. ^{15}N resonances were assigned using a {^{1}H−^{15}N}-HSQC spectrum[48] acquired at 288 K and 500 MHz. The {^{1}H−^{15}N}-HSQC spectrum of the selectively ^{15}N-labeled *N*-acetyl-Hir(55−65) peptide again did not show a detectable population of a potential cis isomer for residue Pro60, in agreement with the conclusions established previously using proton NMR spectroscopy (Ni et al., 1993[44] and references therein).

The sample temperatures were calibrated using methanol.[48] The core of the ^{15}N NMR relaxation dispersion measurements is the relaxation-compensated CPMG pulse sequence (Figure 1).[40,41] In the t_1 (^{15}N) dimension, 32 complex data points were acquired with a spectral width of 4.6 ppm for both the 500 and 800 MHz data sets. In the t_2 (^{1}H) dimension, 1024 complex data points were collected with spectral widths of 5000 Hz at 500 MHz and 7183.91 Hz at 800 MHz. Data matrices were zero-filled to 4096 and 512 prior to Fourier transformation. A Gaussian weighting function was used in both dimensions. The integral intensities of the {^{1}H−^{15}N}-HSQC peaks were obtained using the NLinLs program.[49] The windows for peak integration were normally 15(F2) × 25(F1) points at 500 MHz and 12(F2) × 20(F1) points at 800 MHz. In some cases, smaller windows were used for peak integration or 6(F2) × 16(F1) points at 500 MHz and 4(F2) × 12(F1) points at 800 MHz (see Results section for more details).

Two-site exchange and three-site exchange equations describing the evolution of magnetization under a CPMG echo train were integrated numerically and fit to the experimental NMR data with the use of MatLab (Mathworks).[55,56] Under the experimental conditions, complex magnetization **M** in the rotating frame was assumed to evolve between the refocusing pulses according to

$$d\mathbf{M}/dt = (\mathbf{R} + \mathbf{R}_{EX})\mathbf{M} \tag{1}$$

where

$$\mathbf{R} = \begin{pmatrix} -R_{2b} - i\delta\omega_{b2} & 0 & 0 \\ 0 & -R_{2b} - i\delta\omega_{b1} & \\ 0 & 0 & R_{2f} - i\delta\omega_f \end{pmatrix} \tag{1a}$$

$$\mathbf{R}_{EX} = \begin{pmatrix} -k_1 - k_{off}{}^2 & k_2 & k_{on}{}'^2 \\ k_1 & -k_2 - k_{off}{}^1 & k_{on}{}'^1 \\ k_{off}{}^2 & k_{off}{}^1 & -k_{on}{}'^1 - k_{on}{}'^2 \end{pmatrix} \tag{1b}$$

for a three-site exchange model, and

$$\mathbf{R} = \begin{pmatrix} -R_{2b} - i\delta\omega_b & 0 \\ 0 & -R_{2f} - i\delta\omega_f \end{pmatrix} \tag{1c}$$

$$\mathbf{R}_{EX} = \begin{pmatrix} -k_{off} & k_{on}{}' \\ k_{off} & -k_{on}{}' \end{pmatrix} \tag{1d}$$

for a two-site exchange model.[55] The notation for exchange rate constants is shown in Figure 2. In the cases of "linear" (Figure 2C) or "forked" (Figure 2D) three-state exchange schemes rate constants between nonexchanging species ($k_{on}{}'^2$, $k_{off}{}^2$ or k_1, k_2, respectively) were set to zero. R_{2b} and R_{2f} are the intrinsic transverse relaxation rates for the peptide ^{15}N nuclei in the bound and free forms, respectively. The transverse relaxation rates for the bound peptide in two possible complexes are assumed to be equal in our current analysis. Variables $\delta\omega_{b2}$ and $\delta\omega_{b1}$ are the resonance frequency offsets ($\omega - \omega_0$) for the corresponding bound states, $\delta\omega_f$ is the resonance frequency offset for the free peptide, and ω_0 is the angular frequency of the CPMG RF pulse train.

(49) Delaglio, F.; Grzesiek, S.; Vuister, G. W.; Zhu, G.; Pfeifer, J.; Bax, A. *J. Biomol. NMR* **1995**, *6*, 277−293.
(50) Gullion, T.; Baker, D. B.; Conradi, M. S. *J. Magn. Reson.* **1990**, *89*, 479−484.
(51) Piotto, M.; Saudek, V.; Sklenar, V. *J. Biomol. NMR* **1992**, *2*, 661−665.
(52) Shaka, A. J.; Barker, P. B.; Freeman, R. *J. Magn. Reson.* **1985**, *64*, 547−552.
(53) Marion, D.; Ikura, M.; Tschudin, R.; Bax, A. *J. Magn. Reson.* **1989**, *85*, 393.
(54) Blackledge, M. J.; Bruschweiler, R.; Griesinger, C.; Schmidt, J. M.; Xu, P.; Ernst, R. R. *Biochemistry* **1993**, *32*, 10960−10974.
(55) Jen, J. *J. Magn Reson.* **1978**, *30*, 111−128.
(56) Tollinger, M.; Skrynnikov, N. R.; Mulder, F. A.; Forman-Kay, J. D.; Kay, L. E. *J. Am. Chem. Soc.* **2001**, *123*, 11341−11352.

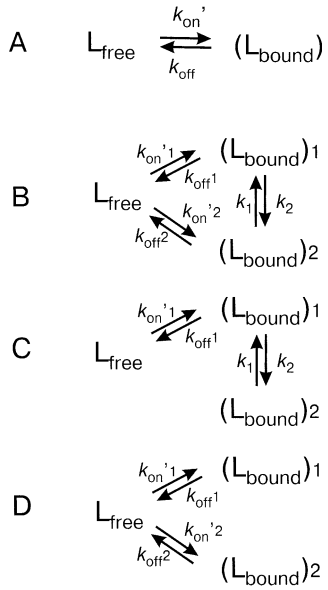

Figure 2. Hypothetic pseudo-first-order two-site and three-site exchange mechanisms for the interaction of *N*-acetyl-Hir(55−65) with human prothrombin. Addition of an extra bound state to the two-state exchange model (a) produces a "full" three-site exchange model (b) with two additional exchange pathways. "Full" three-site exchange scheme turns into "linear" (c) and "forked" (d), if the corresponding absent exchange pathways are too slow to be sensed by NMR.

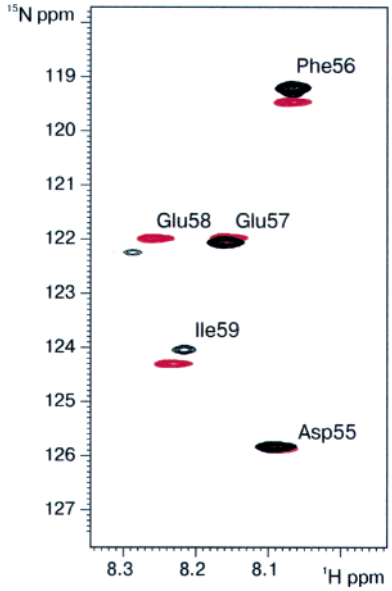

Figure 3. Overlaid {^{1}H−^{15}N}-HSQC spectra of the *N*-acetyl-Hir(55−65) peptide in the absence (red) and presence (black) of human prothrombin. The peptide was dissolved at ∼1.5 mM in an aqueous solution that was 50 mM in NaCl and 50 mM in sodium phosphate at pH 5.5. An aliquot of human prothrombin solution (∼0.3 mM) was added to the peptide solution to produce a prothrombin/peptide molar ratio of ∼1:30. The spectra were recorded at 500 MHz and at 298 K.

The programs for data fitting were adapted from a MatLab script for a "linear" three-state exchange scheme,[56] which was kindly provided by Lewis E. Kay at the University of Toronto. Values for k_{off}, k_{on}', k_{off}^1, k_{off}^2, $k_{on}'^1$, k_1, k_2, R_{2b}(500 MHz), R_{2b}(800 MHz), $\delta\omega_b$, $\delta\omega_{b1}$, and $\delta\omega_{b2}$ (Figure 2) were fitted as independent variables. Values $k_{on}'^2$, p_b, p_{b1}, p_{b2}, and $p_f = (1 - p_{b1} - p_{b2})$, with p standing for the population of the corresponding species, were derived using the condition of microscopic reversibility $k_{ij}p_i = k_{ji}p_j$,[55] where k_{ij} denotes the exchange rate constant for the transformation of species i into species j. R_{2f}, or the R_2 relaxation rate of the peptide ^{15}N nuclei in the free state as defined by the CPMG pulse sequence (Figure 1), and $\delta\omega_f$ were determined experimentally for a sample of the peptide alone under the same experimental conditions. Three matrices $\mathbf{R}_{EX}$(1:45), $\mathbf{R}_{EX}$(1:35), and $\mathbf{R}_{EX}$(1:30) for each prothrombin/peptide ratio were used to fit simultaneously the relaxation dispersion curves at three prothrombin concentrations. Matrices $\mathbf{R}_{EX}$(1:35) and $\mathbf{R}_{EX}$(1:30) were produced from $\mathbf{R}_{EX}$(1:45) by substituting exchange rates k_{on}' (or $k_{on}'^1$ and $k_{on}'^2$ in the models with two dissociation routes) with $1.29 \times k_{on}'$ (or $1.29 \times k_{on}'^1$ and $1.29 \times k_{on}'^2$) and $1.5 \times k_{on}'$ (or $1.5 \times k_{on}'^1$ and $1.5 \times k_{on}'^2$), respectively. The ratios 1.29 and 1.5 for $\mathbf{R}_{EX}$(1:35) and $\mathbf{R}_{EX}$(1:30) reflect the increase of prothrombin concentration in the relationship $k_{on}' = k_{on}[E_f]$ under the assumption of $[L_{free}] \gg K_D$ and $[L_0] \gg [E_0]$ (see eqs 2a−c) and were obtained using the volumes of the added prothrombin solution in the titration. The populations of different species with increased prothrombin concentrations were recalculated in accordance with the modified k_{on}' (or $k_{on}'^1$ and $k_{on}'^2$) values.

The errors of fitting were estimated through Monte Carlo analysis. For each of 200 Monte Carlo samples, random deviations of the measured peak integral intensities were generated. The absolute value of the deviation was set to 1% of the intensity corresponding to zero relaxation delay (I_0), which was a justifiable uncertainty based on a few independent experiments. The integral intensity of I_0 did not deviate by more then 1% from its average value when measured before and after the series of CPMG experiments, and the low-field part of the relaxation dispersion profiles did not deviate by more than ∼0.5 s^{-1} in repeated experiments. Error analysis for the single exponential approximation was carried out in a slightly different manner. The standard deviations of the fitted parameters were estimated through (bootstrap) Monte Carlo simulations[57] using a maximum deviation of ±10% for all experimental R_2 values.

Results

The peptide *N*-acetyl-*Asp-*Phe-*Glu-*Glu-*Ile-Pro-Glu-Glu-Tyr-Leu-Gln (to be referred to as *N*-acetyl-Hir(55−65)), containing five ^{15}N-labeled residues, Asp_{55}, Phe_{56}, Glu_{57}, Glu_{58} and Ile_{59}, at their backbone amide nitrogens, displays in solution slowly relaxing (sharp) proton and ^{15}N NMR signals with no detectable response of the ^{15}N transverse relaxation rate to the changes in CPMG pulse rate. Upon addition of a small amount of prothrombin, four of the five {^{1}H−^{15}N}-HSQC peaks were found to shift and broaden (Figure 3). For all exchange regimes, excess ligand over a large protein−ligand complex guarantees that the NMR spectrum is dominated by the slowly decaying signals resulting from the free ligand.[58] The ^{15}N transverse relaxation dispersion data (Figure 4) were collected using our implementation (Figure 1) of the constant-time ^{15}N CPMG experiment[42] along with additional CPMG elements for sensitivity enhancement of exchange-broadened signals[59] and for the compensation of heating effects[60] caused by the CPMG pulses.[61] The use of compensating ^{15}N CPMG pulses was found to be critical for running the relaxation dispersion experiments on a very high field NMR spectrometer (such as at 800 MHz) that may be very sensitive to small temperature fluctuations.

Figure 4 shows the ^{15}N relaxation dispersion of the backbone amide nitrogen atoms of residues Phe_{56}, Glu_{57}, Glu_{58}, and Ile_{59} of *N*-acetyl-Hir(55−65) in the presence of human prothrombin.

(57) Press, W. H.; Teukolsky, S. A.; Vetterling, W. T.; Flannery, B. P. In *Numerical Recipes in Fortran*; Cambridge University Press: New York, 1992.
(58) Ni, F. *Prog. Nucl. Magn. Reson. Spectrosc.* **1994**, *26*, 517−606.
(59) Mulder, F. A. A.; Spronk, C. A. E. M.; Slijper, M.; Kaptein, R.; Boelens, R. *J. Biomol. NMR* **1996**, *8*, 223−228.
(60) Wang, A. C.; Bax, A. *J. Biomol. NMR* **1993**, *3*, 715−720.
(61) Mulder, F. A.; van Tilborg, P. J.; Kaptein, R.; Boelens, R. *J. Biomol. NMR* **1999**, *13*, 275−288.

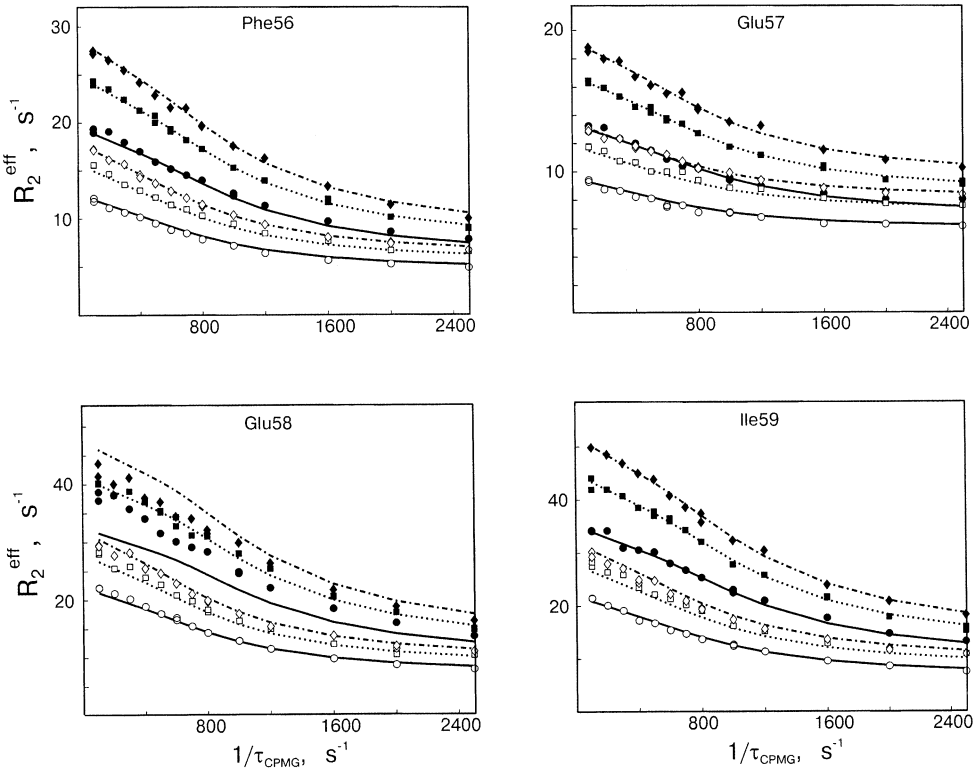

Figure 4. ^{15}N relaxation dispersion curves for the ^{15}N-labeled peptide *N*-acetyl-Hir(55−65) in complex with human prothrombin. The peptide was ∼1.5 mM in an aqueous solution that was 50 mM in NaCl and 50 mM in sodium phosphate at pH 5.5 and at 25 C°. The dispersion curves were recorded at three prothrombin/peptide ratios, 1:45 (○, ●), 1:35 (□, ■), and 1:30 (◇, ◆), and at two ^{15}N frequencies, 50.684 MHz (○, □, and ◇) and 81.076 MHz (●, ■, and ◆). The ^{15}N dispersion curves were fitted to a two-site exchange scheme separately for each residue but simultaneously for all three prothrombin/peptide ratios. The fitted curves are shown as a solid line at 1:45, dotted line at 1:35, and dash−dot line at 1:30 prothrombin/peptide ratios.

The amide nitrogen of Asp_{55} had rather sharp proton and ^{15}N NMR signals (Figure 3) and showed very little relaxation dispersion, in agreement with the very little binding-induced line broadening of its amide proton resonance,[44] and therefore is not included in further analysis. Three prothrombin/peptide molar ratios were used, namely ∼1:45, ∼1:35, and ∼1:30. The accuracy of the absolute peptide or prothrombin concentrations was not critical for the data analysis, as only the increases in the prothrombin/peptide ratio, measured by the volume of the added prothrombin stock solution, need to be included in the data fitting process (vide infra). The approximate prothrombin concentrations were used only to discriminate physically reasonable from unreasonable fits. In the course of the titration, the volumes of the added prothrombin solution after the second and third additions were 1.29 and 1.5 times that of the first addition, respectively. The relaxation dispersion data were fitted using numerical calculation of magnetization evolution during the ($\tau_{CPMG}/2 - 180° - \tau_{CPMG} - 180° - \tau_{CPMG}/2$) element of the CPMG sequence.[55,56]

Two-Site Exchange Model. At first, a two-site exchange model was assumed according to the scheme shown in Figure 2a and fitted independently for every ^{1}H/^{15}N cross-peak. In this scheme, p_b is the bound population of the peptide, $\delta\omega_{bf} = (\delta\omega_b - \delta\omega_f)$ is the ^{15}N resonance peak separation between the bound and the free states, R_{2f} is the transverse relaxation rate for the free peptide, R_{2b} is the transverse relaxation rate for the bound peptide, k_{off} is the dissociation rate constant, and k_{on}' stands for $k_{on}[E_f]$, where k_{on} is the association rate constant and $[E_f]$ is the concentration of the free prothrombin. In turn, the concentration of the free prothrombin is defined by the concentration of the free peptide $[L_{free}]$, the total concentration of added prothrombin $[E_0]$, and the equilibrium dissociation constant $K_D = k_{off}/k_{on}$ as

$$[E_f] = [E_0]K_D/(K_D + [L_{free}]) \qquad (2a)$$

which, in the case of $[L_{free}] \gg K_D$, is proportional to the $[E_0]/[L_{free}]$ ratio. If also $[L_0] \gg [E_0]$, which is normally the case for this type of experiment, then

$$[E_f] \approx [E_0]K_D/[L_0] \qquad (2b)$$

$$k_{on}'(\text{second}) = [(V_1 + V_2)/V_1] \times k_{on}'(\text{first}) \qquad (2c)$$

where k_{on}'(first) and k_{on}'(second) are the pseudo-first-order association rate constants after the first and the second additions of prothrombin and V_1 and V_2 are the volumes of the prothrombin solution used in the first and second additions of prothrombin, respectively. Furthermore, eqs 2a−c are valid for any exchange mechanism, for example, all those of Figure 2, except that K_D is not generally equal to k_{off}/k_{on}.

A least-squares fitting procedure was used to extract k_{off}, p_b, $\delta\omega_{bf}$, and the values of R_{2b} at the two magnetic fields. The results of the fits using full matrix analysis (eqs 1c and 1d) are presented in Table 1. Essentially the same results were also obtained when the relaxation dispersion data were fitted (Table 1) using the single-exponential approximation of the two-state model.[30,41,55,62] All the variable parameters obtained by both methods were identical within the experimental error limits (Table 1). It is seen that the behavior of residues Phe_{56} and Ile_{59} is consistent with a two-site exchange model. Both residues display highly similar k_{off} values with the R_{2b} values independent

(62) Carver, J. P.; Richards, R. E. *J. Magn. Reson.* **1972**, *6*, 89−105.

Table 1. Kinetic and ^{15}N Relaxation Dispersion Parameters of the *N*-Acetyl-Hir(55−65) Peptide in Complex with Human Prothrombin for a Two-Site Exchange Scheme[a]

residue	k_{off}, s^{-1}	$\delta\omega_{bf}$, ppm	p_b, %	R_{2b} [R_{2b}(800)], s^{-1}	R_{2f} [R_{2f}(800)], s^{-1}
Phe56/1	2030 ± 110	−3.7 ± 0.2	2.01 ± 0.14	161 ± 8 [319 ± 22]	1.38 [0.95]
Phe56/*	2050 ± 146	−3.6 ± 0.2	2.0 ± 0.2	155 ± 11 [308 ± 30]	
Phe56/2	2015 ± 110	−3.9 ± 0.2	2.40 ± 0.21	199 ± 10 [304 ± 21]	
Phe56/3	2150 ± 105	−4.2 ± 0.2	2.53 ± 0.15	190 ± 7 [304 ± 18]	
Phe56	2080 ± 60	−4.0 ± 0.1	1.80 ± 0.06	188 ± 5 [308 ± 11]	
Glu57/1	1540 ± 180	2.6 ± 0.3	1.74 ± 0.20	310 ± 35 [460 ± 60]	1.60 [1.44]
Glu57/*	1570 ± 209	2.6 ± 0.4	1.7 ± 0.3	310 ± 46 [454 ± 78]	
Glu57/2	1820 ± 190	3.4 ± 0.3	1.74 ± 0.16	410 ± 40 [514 ± 54]	
Glu57/3	2030 ± 200	3.5 ± 0.4	1.92 ± 0.21	400 ± 40 [513 ± 58]	
Glu57	1850 ± 110	3.2 ± 0.2	1.36 ± 0.08	390 ± 20 [510 ± 35]	
Glu58/1	2260 ± 100	4.2 ± 0.2	3.42 ± 0.20	136 ± 6 [255 ± 17]	2.14 [2.53]
Glu58/1/w	2150 ± 90	4.0 ± 0.2	3.71 ± 0.24	142 ± 6 [268 ± 17]	
Glu58/*	2437 ± 153	4.3 ± 0.3	3.2 ± 0.3	132 ± 9 [245 ± 24]	
Glu58/2	1790 ± 80	5.4 ± 0.2	3.09 ± 0.12	233 ± 7 [339 ± 14]	
Glu58/2/w	2130 ± 80	4.8 ± 0.2	3.73 ± 0.18	178 ± 6 [279 ± 14]	
Glu58/3	1680 ± 80	5.3 ± 0.2	3.34 ± 0.14	259 ± 7 [367 ± 14]	
Glu58/3/w	2210 ± 90	4.3 ± 0.3	4.86 ± 0.39	160 ± 7 [248 ± 17]	
Ile59/1	2060 ± 90	−4.4 ± 0.2	3.04 ± 0.15	209 ± 7 [361 ± 18]	0.71 [1.03]
Ile59/*	2165 ± 153	−4.5 ± 0.3	3.0 ± 0.2	206 ± 11 [351 ± 27]	
Ile59/2	2020 ± 80	−4.9 ± 0.2	3.55 ± 0.15	260 ± 8 [340 ± 15]	
Ile59/3	2260 ± 100	−4.5 ± 0.2	4.41 ± 0.28	193 ± 8 [312 ± 18]	
Ile59	2160 ± 60	−4.6 ± 0.1	2.90 ± 0.10	221 ± 5 [330 ± 10]	
56/57/59[b]	2470 ± 40		2.40 ± 0.05	193 ± 4 [245 ± 6]	

[a] The fitted parameters k_{off}, $\delta\omega_{bf}$, p_b, and R_{2b} represent, respectively, the dissociation rate constant of the protein−peptide complex, the frequency separation for a peptide ^{15}N signal in the free and bound states $\delta\omega_{bf} = (\delta\omega_b - \delta\omega_f)$, the apparent fraction of the bound peptide, and the apparent R_2 relaxation rate of the peptide ^{15}N nuclei in the bound state. Signs of the $\delta\omega_{bf}$ values are derived from the signs of the prothrombin-induced chemical shifts for the corresponding {^{1}H−^{15}N}-HSQC cross-peaks. The listed values R_{2b} are those at 500 MHz (with an ^{15}N frequency of 50.684 MHz), and the values in the square brackets are those at 800 MHz (^{15}N frequency: 81.076 MHz). The values of R_{2f}, or the intrinsic R_2 relaxation rate of the peptide ^{15}N nuclei in the free state, were determined experimentally for a sample of the peptide in the absence of prothrombin under the same experimental conditions and using the same pulse sequence (Figure 1) and were found independent of the CPMG pulse rate. Residues were fitted independently except for the last row designated as 56/57/59. For every amino acid residue, rows denoted /1, /2, and /3 correspond to data sets at prothrombin/ligand ratios of ∼1:45, ∼1:35, and ∼1:30, respectively. Rows denoted /w correspond to the parameters using relaxation dispersion profiles of Glu_{58} obtained with a smaller integration window (see text). Rows denoted /* show the results of the fitting of the data in rows denoted /1 (∼1:45 prothrombin/peptide ratio) using the single-exponential approximation.[30,55,62] The last row for every residue, except for Glu_{58} which strongly deviates from the expected concentration dependence, lists parameters obtained by a simultaneous fit to dispersion data at all three prothrombin concentrations, with the value in the p_b column corresponding to the prothrombin/ligand ratio of ∼1:45. The row 56/57/59 displays parameters for the simultaneous fit to the relaxation dispersion of all three residues Phe_{56}, Glu_{57}, and Ile_{59} at three prothrombin concentrations. [b] Fitted values of $\delta\omega_{bf}$ were −3.1 ± 0.1, 1.9 ± 0.8, and −5.5 ± 0.1 ppm, for residues Phe_{56}, Glu_{57}, and Ile_{59}, respectively.

of the peptide/protein ratio and p_b growing roughly comparable with the amount of the added prothrombin. On the other hand, Glu_{57} displays some growth of k_{off} and only a slight increase in p_b upon the incremental growth of the prothrombin concentration. In addition, R_{2b} values for Glu_{57} at both fields appear to be unusually high, almost doubling the values calculated for other ^{15}N sites. Glu_{58} had a noticeably unusual behavior: the calculated k_{off} value decreases with the addition of prothrombin, while R_{2b} increases, and p_b is not changing. Regardless, fitting results with residues Phe_{56} and Ile_{59} indicate that ^{15}N-relaxation dispersion data at two magnetic fields and at a single prothrombin concentration can uniquely determine the five unknown parameters, k_{off}, p_b, $\delta\omega_{bf}$, R_{2b}(500), and R_{2b}(800), describing two-state binding.

The signs of the $\delta\omega_{bf}$ values shown in Table 1 were assigned according to the observed cross-peak shifts induced by prothrombin titration (Figure 3). Under the condition of $p_f \gg p_b$, binding-induced ^{15}N resonance shifts correlate with the relaxation and kinetic exchange parameters according to the formulation of Swift and Connick,[63] which for a two-site exchange situation are expressed analytically as follows:

$$\Delta\omega_{obs} = k_{on}' k_{off}\, \delta\omega_{bf}/[(k_{off} + R_{2b})^2 + (\delta\omega_{bf})^2] \qquad (3)$$

where $\Delta\omega_{obs}$ is the observed shift of an ^{15}N resonance peak induced by prothrombin binding. These binding-induced resonance shifts are normally small (∼0.03−0.3 ppm) (Figure 3), and their signs can be derived with certainty from comparison of the {^{1}H−^{15}N}-HSQC spectra of the peptide free and in the presence of a subequivalent of prothrombin. Theoretically, therefore, experimental measurements of the observed shift differences, $\Delta\omega_{obs}$, can provide supplementary information for use as constraints (by use of eq 3) as part of the data fitting process.[33] In practice, however, it may not be advisable to attempt quantitative measurements of $\Delta\omega_{obs}$ due to the sensitivity of the HSQC spectrum of the peptide to the slightest changes in pH and salt concentrations and to the additions of the binding protein prothrombin. These minor uncertainties in the solution conditions have little effect on the intrinsic NMR relaxation and kinetic parameters but may result in spectral shifts of up to ∼0.05−0.08 ppm for the ^{15}N resonances of the peptide (data not shown). In practice, the derived values of $\delta\omega_{bf}$ can be further verified by a comparison of the binding-induced resonance shifts obtained at different field strengths, since, according to eq 3, a higher magnetic field would decrease the observed resonance shift when expressed in ppm.

We then carried out a simultaneous fit of the dispersion curves at all three prothrombin concentrations, using the fact that k_{on}' is proportional to $[E_f]$ and, hence, to $[E_0]/[L_0]$ (eqs 2a−c). The fit was performed independently for each ^{1}H/^{15}N cross-peak (Figure 4 and Table 1). As expected, the fitted dispersion curves for Phe_{56} and Ile_{59} were in a good agreement with the two-site exchange model. It was also possible to fit reasonably well the

(63) Swift, T. J.; Connick, R. E. *J. Chem. Phys.* **1962**, *37*, 307−320.

dispersion curves of Glu_{57} using the same model. Again, for Glu_{57}, fitted R_{2b} values were higher, while p_b was smaller than expected (Table 1). It is important to emphasize that the apparent transverse relaxation rate was very sensitive to the increase of $[E_0]/[L_0]$ for every pair of the dispersion curves with the addition of prothrombin. It was therefore easy to verify the linearity of $[E_f]$ growth with the addition of prothrombin simply by including it as a fitted parameter. For Phe_{56}, Glu_{57}, and Ile_{59} ^{15}N sites, fitted $[E_f]_1/[E_f]_2$ values for every pair of prothrombin concentrations were in excellent agreement with the relative volumes of the prothrombin solution added or the $([E_0]/[L_0])_1/([E_0]/[L_0])_2$ ratio (data not shown). This observation is consistent with the previous reports demonstrating that K_D for the binding of *N*-acetyl-Hir(55−65) with prothrombin is of the order of ∼100−300 μM[44,45] and, therefore, is significantly less than the peptide concentration (∼1.5 mM).

Simultaneous fitting of eighteen dispersion curves at the three concentrations of prothrombin for all three residues Phe_{56}, Glu_{57}, and Ile_{59} was also performed and is listed in the last row of Table 1. For this particular fit, we assumed equal R_{2b} values for each residue in the bound state to simplify the calculations. Whereas calculated parameters were close to those obtained independently for residues Phe_{56} and Ile_{59}, the quality of the fit for residues Phe_{56} and Glu_{57} declined (data not shown), and the fit forced poor convergence of the parameter $\delta\omega_{bf}$ (1.9 ± 0.8 ppm) for Glu_{57}.

It was not possible to obtain a reasonable fit for residue Glu_{58} using a two-site exchange model at three prothrombin concentrations (Figure 4). The apparent transverse relaxation rate of Glu_{58} does not grow rapidly enough with the addition of prothrombin. Apparently, this observation is related to the inherent difficulties in the quantitative integration of the Glu_{58} cross-peak, which displays the highest prothrombin-induced broadening among all HSQC peaks (Figure 3). In addition, inspection of the $\{^1H-^{15}N\}$-HSQC spectra at low CPMG pulse rate and the highest prothrombin concentration indicated that there appears to be a CPMG pulse rate-independent contribution to the measured Glu_{58} magnetization from a very weak overlapping peak. To verify this, we quantitated the cross-peak of Glu_{58} using a smaller integration window [6(F2) × 16(F1) points at 500 MHz and 4(F2) × 12(F1) points at 800 MHz] and obtained a more reasonable concentration dependence of the CPMG relaxation dispersion and fitted parameters (Table 1). Quantitation of other peaks with the smaller window yielded unchanged relaxation dispersion profiles within the limits of the experimental error (data not shown). These observations indicate that the very weak and slowly relaxing resonance overlapping with Glu_{58} cannot be from a minor conformation of the peptide as a result of any significant population of a potential cis isomer for residue Pro_{60} (also see Materials and Methods). However, considering the ambiguity of the derived relaxation parameters for Glu_{58}, we did not include the relaxation dispersion curves of Glu_{58} in the following three-site exchange analysis.

Three-Site Exchange Model. The relaxation behavior of residue Glu_{57} suggests the presence of other conformations in the bound state. Although the relaxation dispersion of Glu_{57} can be fitted by a two-site exchange model at all three prothrombin concentrations, the abnormally high values of R_{2b} as well as comparatively low values of p_b, might be artifacts originating from the presence of additional exchange pathways. In fact, even residues Phe_{56} and Ile_{59} display R_{2b} values somewhat higher than expected, if we assume that in the bound state it is the motions of the complex as a whole that define the transverse relaxation of the ligand. We estimated theoretical values of R_2 for a protein with the molecular mass of prothrombin (72 kDa) and order parameter $S = 0.8$ and 1.0 to be, respectively, 95/122 and 119/153 s^{-1} at 500/800 MHz.[64] Therefore, we are interested in how including an additional bound state in the analysis of the experimental dispersion curves would affect the calculated values of R_{2b}, p_b, and k_{off}.

In the most general case, including an additional bound state adds two kinetic pathways to the model (Figure 2B). One pathway is the kinetic exchange on the surface of the protein, that can be a consequence of both protein and peptide conformational conversions. Another pathway is an alternative association−dissociation route of the distinct bound species, formally producing an additional pair of k_{off} and k_{on} rate constants. If one of the two pathways is too slow to influence the relaxation, the system obeys either "linear" three-state behavior (Figure 2C) or "forked" three-state behavior (Figure 2D). In our evaluation, we assumed that the transverse relaxation rate R_{2b} for both bound states are equal. This way, there are a total of nine independent parameters describing the general three-site exchange, while the total number of the degrees of freedom is reduced by one for the "linear" or "forked" three-site exchange mechanisms (Figure 2 and eq 1). The increment of the prothrombin concentration during the titration does not increase the total degrees of freedom as long as the volume ratios of the titrated prothrombin are known accurately (see Materials and Methods). In principle, therefore, the nine kinetic and NMR relaxation parameters may be obtained from the fitting of only two dispersion data sets at two different prothrombin concentrations.

In practice, we found that the three-state system may be somewhat underdefined, and depending on the starting conditions, the calculation converged to a few clusters of fitted parameters. The clusters were filtered on the basis of physical feasibility, and parameter sets containing negative rate constants or relaxation times, as well as $p_b = p_{b1} + p_{b2}$ exceeding or comparable with $p_{free} = (1 - p_b)$, were not considered. To fit the experimental dispersion curves of Glu_{57} to a "linear" three-site model (Figure 2C), it was necessary to use simultaneously the six dispersion curves for the three concentrations of prothrombin recorded at two different magnetic fields to obtain convergent results. Dependent on the starting conditions for iterative fitting, the fitted parameters in the calculations converged either to the two-site exchange mechanism ($k_1 \approx k_2 \approx 0$) or to the actual linear three-site exchange mechanism ($k_1 = 50 \pm 30$ s^{-1}, $k_2 = 150 \pm 70$ s^{-1}). The resulting three-site exchange parameters (Table 2) were, in fact, not so much different from those of the two-site exchange, since the population of the dissociation-competent bound state, p_{b1}, was found to be 1.3 ± 0.1%, close to that found for the two-site mechanism (Table 1). Part of the bound peptide was redistributed into the $(L_{bound})_2$ state ($p_{b2} = 4.0 \pm 1.8\%$), thus increasing the total bound peptide population. Notably, the k_{off} value (2090 ± 230 s^{-1}) was close to that of residues Phe_{56} and Ile_{59} found

(64) Luginbuhl, P.; Wuthrich, K. *Prog. Nucl. Magn. Reson. Spectrosc.* **2002**, *40*, 199−247.

Table 2. Kinetic and ^{15}N Relaxation Dispersion Parameters of the *N*-Acetyl-Hir(55−65) Peptide in Complex with Human Prothrombin for a Three-Site Exchange Scheme[a]

model	residue	$\delta\omega_{b1f}$, ppm [$\delta\omega_{b2f}$]	k_{off}^1, s^{-1} [k_{off}^2]	k_{off}^{app}, s^{-1}	k_1, s^{-1} [k_2]	k_{ex}, s^{-1}	p_{b1}, % [p_{b2}]	p_b, %	R_{2b}, s^{-1} [R_{2b}(800)]
linear/1	Glu57	3.0 ± 0.5 [6.2 ± 3.0]	2090 ± 230	520 ± 250	50 ± 30 [150 ± 70]	220 ± 80	1.3 ± 0.1 [4.0 ± 1.8]	6.0 ± 1.9	275 ± 50 [370 ± 65]
linear/3	Phe56	−3.1 ± 0.2 [−3.2 ± 0.8]	2710 ± 130	1920 ± 370	480 ± 380 [150 ± 70]	640 ± 430	2.26 ± 0.13 [1.1 ± 0.9]	3.3 ± 0.9	153 ± 13 [205 ± 16]
	Glu57	1.2 ± 1.6 [2.8 ± 5.2]							
	Ile59	−5.7 ± 0.3 [−3.8 ± 2.9]							
circular/3	Phe56	−0.5 ± 2.5 [−2.5 ± 2.0]	2200 ± 1600 [2700 ± 500]	2350 ± 300	60 ± 50 [90 ± 90]	150 ± 130	1.5 ± 1.0 [1.5 ± 0.5]	3.0 ± 0.6	160 ± 25 [205 ± 33]
	Glu57	1.2 ± 1.6 [1.8 ± 1.3]							
	Ile59	−3.1 ± 2.3 [−6.8 ± 1.7]							

[a] $\delta\omega_{b1f}$ and $\delta\omega_{b2f}$ are the frequency separation values for the corresponding ^{15}N signal in the free and bound states $\delta\omega_{b1f} = (\delta\omega_{b1} - \delta\omega_f)$, $\delta\omega_{b2f} = (\delta\omega_{b2} - \delta\omega_f)$. Signs of $\delta\omega_{b1f}$ and $\delta\omega_{b2f}$ are set according to the signs of the prothrombin-induced chemical shifts in the initial parameter list prior to Matlab optimization. Row denoted /1 corresponds to the Monte Carlo samplings performed independently for Glu_{57}, whereas rows denoted /3 correspond to the simultaneous three-site optimizations using data of three residues, Phe_{56}, Glu_{57}, and Ile_{59}. The values in the p_b columns correspond to the prothrombin/ligand ratio of ∼1:45.

in the two-site analysis, while the apparent R_{2b} of Glu_{57} decreased (275 ± 50 and 370 ± 65 s^{-1} at 500 and 800 MHz, respectively) as compared to that in the two-site exchange model (Table 1). Treatment of Glu_{57} as an independent association−dissociation site, undergoing conformational exchange on the protein surface (Figure 2C), yields smaller apparent R_{2b} and larger $p_b = p_{b1} + p_{b2}$ (∼6.0%) values, but it is again not fully consistent with the behavior of Phe_{56} and Ile_{59} sites since the total bound population of Glu_{57} becomes larger than the bound populations for the Phe_{56}/Ile_{59} sites in the two-state analysis. In other words, Glu_{57} appears to spend more time in the "bound" state than Phe_{56} and Ile_{59}, which is not consistent with the applied model. It is worthwhile to note that in the formal three-state exchange description (Figure 2B) the actual separation of "bound" state from "free" state at the residue level is mainly reflected in the large difference between the intrinsic R_{2b} and R_{2f} values. In this respect, although it is easy to imagine a situation when a residue is not interacting (or interacting only weakly) with a prothrombin surface in one of the two bound states in the *N*-acetyl-Hir(55−65)-prothrombin complex, it would still be in the "bound" state, since its R_{2b} would be closer to that dictated by the correlation time of the complex. Within the limits of this definition, dissociation and association of all residues in the peptide occur simultaneously, regardless of their residue-specific behavior on the protein surface.

To "link" the process of association−dissociation between different ^{15}N sites of the peptide, we performed the fitting of all eighteen dispersion curves for the three residues Phe_{56}, Glu_{57}, and Ile_{59} at three concentrations of prothrombin and at two magnetic fields (Figure 5A and Table 2). The experimental curves were in agreement with the "linear" three-site exchange model and yielded $k_{off} = 2710 \pm 130$ s^{-1}, $k_{off}^{app} = 1920 \pm 370$ s^{-1}, $k_1 = 480 \pm 380$ s^{-1}, $k_2 = 150 \pm 70$ s^{-1}, $k_{ex} = k_1 + k_2 = 640 \pm 430$ s^{-1}, $p_{b1} = 2.26 \pm 0.13\%$, $p_{b2} = 1.1 \pm 0.9\%$, $p_b = p_{b1} + p_{b2} = 3.3 \pm 0.9\%$, $R_{2b} = 153/205 \pm 13/16$ s^{-1} at 500/800 MHz. Here, we define $k_{off}^{app} = (p_{b1} \times k_{off}^1 + p_{b2} \times k_{off}^2)/(p_{b1} + p_{b2})$ as an apparent population-weighted dissociation rate for a general three-state system. In the "linear" three-site exchange model, k_{off}^2 is equal to zero, and the expression for k_{off}^{app} becomes $p_{b1} \times k_{off}/(p_{b1} + p_{b2})$. Overall, the "linear" three-site exchange scheme is more consistent with realistic apparent R_{2b} and p_b values than those found in the two-site exchange scheme. Importantly, the calculated k_{off} value was not strongly compromised upon the addition of the second bound state to the model.

The "forked" three-site mechanism (Figure 2D) did not give additional insights in the explanation of experimental results, even if R_{2b} was presumed to be different in the two bound complexes. The fitted curves either did not produce physically meaningful parameters (for example, negative kinetic rate constants and populations were produced) or were similar to the two-site exchange treatment, if k_{off}^1 was assumed to be equal to k_{off}^2 (data not shown).

In a general three-site exchange mechanism, the presence of two dissociation pathways as well as an exchange between two complex conformers is presumed (Figure 2B). Simultaneous fitting of all eighteen dispersion curves for the three residues Phe_{56}, Glu_{57}, and Ile_{59} at three prothrombin concentrations assuming the same kinetic exchange parameters for every ^{15}N peak is shown in Figure 5b. The fitting gave $k_{off}^1 = 2200 \pm 1600$ s^{-1}, $k_{off}^2 = 2700 \pm 500$ s^{-1}, $k_{off}^{app} = 2350 \pm 300$ s^{-1}, $k_1 = 60 \pm 50$ s^{-1}, $k_2 = 90 \pm 90$ s^{-1}, $k_{ex} = k_1 + k_2 = 150 \pm 130$ s^{-1}, $p_{b1} = 1.5 \pm 1.0\%$, $p_{b2} = 1.5 \pm 0.5\%$, $p_b = p_{b1} + p_{b2} = 3.0 \pm 0.6\%$, $R_{2b} = 160/205 \pm 25/33$ s^{-1} at 500/800 MHz (Table 2). The apparent dissociation rate constant k_{off}^{app} has significantly less variability than each of the rate constants k_{off}^1 and k_{off}^2. It means that fitting of the experimental curves may allow a contribution of a state with k_{off} values markedly different from the average, but its contribution to the total bound species is either small or compensated in the averaged dissociation rate. Some of the fits produced result with k_{off}^1 or k_{off}^2 close to zero, which essentially corresponds to a "linear" mechanism.

Parameter Estimation Using Simple Two-Site (On−Off) Binding in the Presence of Alternate Binding Modes. Table 1 and the foregoing discussions indicate that the relaxation dispersion profiles may be treated by a phenomenological two-site binding model describing the peptide−prothrombin interaction. The fitted parameters for some residues, for example, Phe_{56} and Ile_{69}, are in good agreement with physically meaningful two-site models, that is, with reasonable p_b and comparable k_{off} values. Residue Glu_{57}, on the other hand, had a significantly decreased k_{off} value for the two-site model. All residues had somewhat or significantly increased R_{2b} values over what can be expected of a protein−peptide complex with the size of ∼72

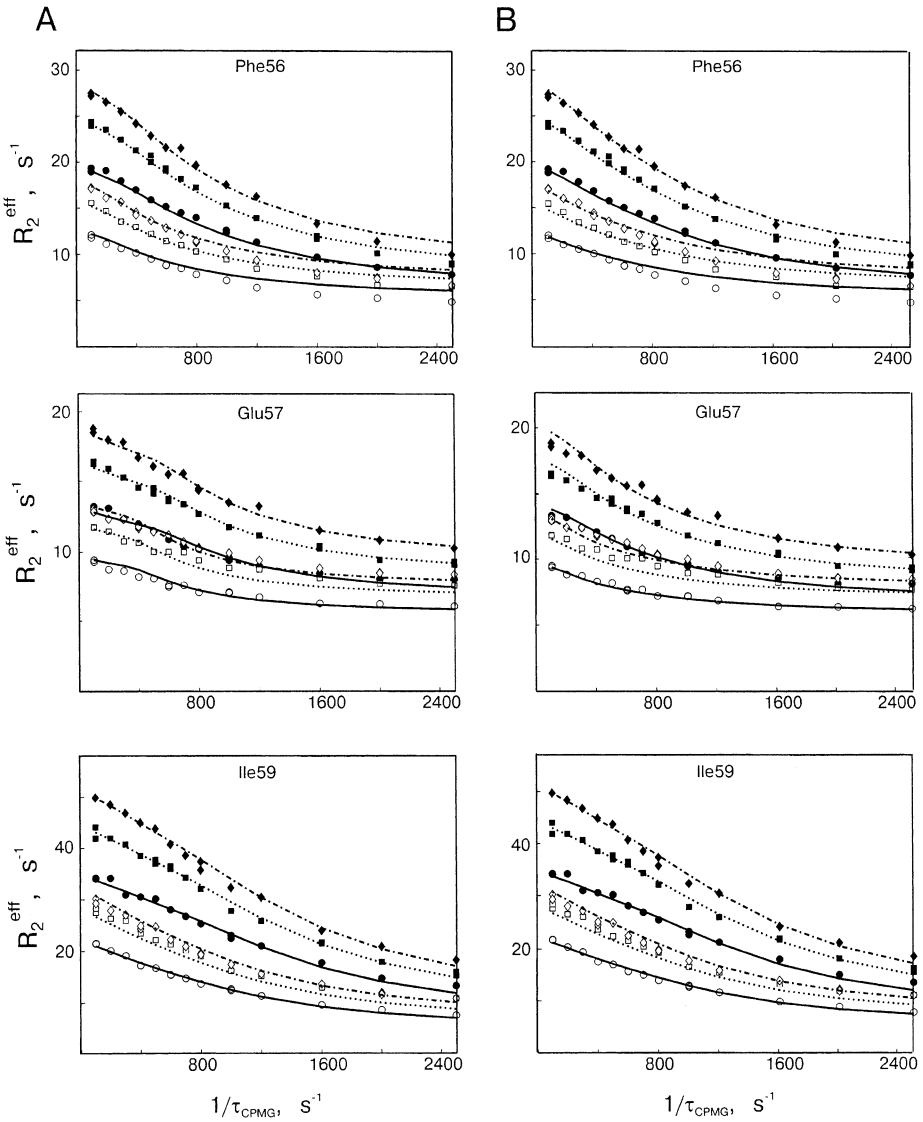

Figure 5. Fits of ^{15}N relaxation dispersion curves for the peptide *N*-acetyl-Hir(55−65) in complex with human prothrombin to three-site exchange schemes. All eighteen curves were fitted simultaneously to experimental data using the (a) "linear" and (b) "full" three-site exchange scheme shown in Figure 2. Experimental conditions and labeling are the same as those in Figure 4.

kDa. The decreased p_b can be understood as resulting merely from the presence of dissociation-incompetent species for the peptide−prothrombin complex by use of the three-site exchange mechanism (Figure 2). For example, for the "forked" model (Figure 2C), implying very slow exchange between the bound species ($k_1 \approx k_2 \approx 0$), the observed magnetization of the free peptide nuclei in the fast CPMG pulsing limit can be shown[30,55] to decay with the following rate constant:

$$R_2^{\text{eff}}(1/\tau_{\text{CPMG}} \rightarrow \infty) = p_f R_{2f} + p_{b1}/(1/R_{2b} + 1/k_{\text{off}}^1) + p_{b2}/(1/R_{2b} + 1/k_{\text{off}}^2) \quad (4)$$

where it is assumed that the two forms of complexes have the same transverse relaxation rates, that is, $R_{2b1} = R_{2b2} = R_{2b}$. In the presence of a dissociation-incompetent species ($k_{\text{off}}^2 \rightarrow 0$), eq 4 becomes, assuming $k_{\text{off}}^1 \gg R_{2b}$,

$$R_2^{\text{eff}}(1/\tau_{\text{CPMG}} \rightarrow \infty) = p_f R_{2f} + p_{b1}/(1/R_{2b} + 1/k_{\text{off}}^1) \approx p_f R_{2f} + p_{b1} R_{2b} \quad (4a)$$

In other words, existence of dissociation-incompetent conformations reduces the apparent p_b to the value of p_{b1}.

Figure 6 shows the effect of introducing exchange, that is, the increase of k_1 and k_2, between the two bound conformations, one of which is dissociation-incompetent ($k_{\text{off}}^2 = 0$). Indeed, the absence of a slow conformational exchange gives rise to reduced plateau values of the dispersion profile, as predicted by eq 4a. As the rates of conformational exchange go up, there is a general increase of the transverse relaxation rates of the peptide at all repetition rates of the CPMG pulse. At a very slow rate of conformational exchange ($k_{ex}/2 = k_1 = k_2 = 1$ s^{-1}), the extracted kinetic and relaxation parameters were, as expected, practically identical to the parameters of fast exchange involving only one bound conformation, $(L_{bound})_1$. With the increase in k_{ex}, the low-pulsing part of the relaxation dispersion profiles is also affected for both ^{15}N frequencies but is more sensitive to the slow exchange at the lower ^{15}N frequency (50.6 MHz). This perturbation is manifested as an apparent decrease in k_{off}, a further decrease in p_b, and a large increase in R_{2b} (Table 3). The always opposing and partly compensatory changes in

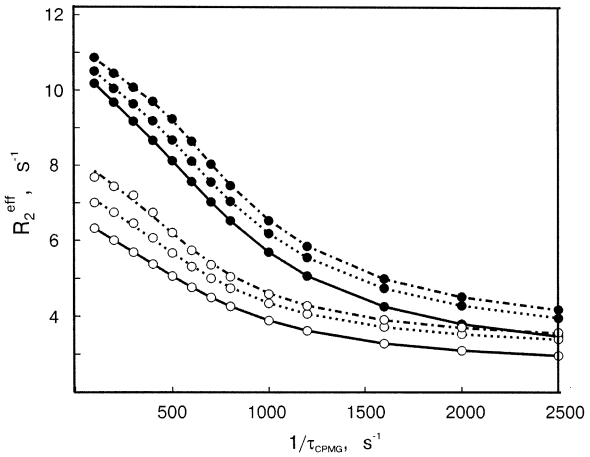

Figure 6. Influence of the slow conformational exchange in fast-dissociating peptide−protein complexes on the peptide relaxation dispersion profile. The three pairs of the "experimental" data correspond to three different values of $k_{ex} = k_1 + k_2$, which were generated using the linear three-site model (Figure 2c) and eqs 1 at two ^{15}N frequencies, 50.6 MHz (○) and 81.1 MHz (●). The best fits to the two-site exchange model are shown as pairs of solid lines ($k_{ex} = 2$ s^{-1}), dotted lines ($k_{ex} = 200$ s^{-1}), and dash−dotted lines ($k_{ex} = 400$ s^{-1}). Only the k_{ex} was altered, whereas other parameters were kept constant at $p_{b1} = p_{b2} = 1.22\%$, $k_{off} = 2000$ s^{-1}, $R_{2f}(500) = 1.60$ s^{-1}, $R_{2f}(800) = 1.44$ s^{-1}, $R_{2b}(500) = 95$ s^{-1}, $R_{2b}(800) = 119$ s^{-1}, $\delta\omega_f = 0.0$ ppm, $\delta\omega_{b1} = 3.0$ ppm, and $\delta\omega_{b2} = 6.0$ ppm.

Table 3. Extracted Two-Site Exchange Kinetic and Relaxation Dispersion Parameters for a Peptide ^{15}N Site Involved in a "Linear" Three-Site Exchange Mechanism (Figure 6)[a]

k_{ex}, s^{-1}	p_{b1} [p_{b2}], %	k_{off}, s^{-1}	$\delta\omega_{bf}$, ppm	p_b, %	R_{2b} [R_{2b}(800)], s^{-1}
2	1.22 [1.22]	1998	3.00	1.233	96 [120]
200	1.22 [1.22]	1715	3.49	1.074	159 [198]
400	2.00 [0.44]	1755	3.51	1.726	129 [162]
400	1.64 [0.80]	1598	3.77	1.381	154 [194]
400	1.22 [1.22]	1452	3.96	1.046	186 [233]
400	0.80 [1.64]	1336	4.05	0.719	229 [286]
400	0.44 [2.00]	1261	4.02	0.419	287 [354]

[a] The parameters k_{off}, $\delta\omega_{bf}$, p_b, and R_{2b} are the apparent kinetic and relaxation parameters obtained by fitting "experimental points", which were generated using a "linear" three-site model (Figure 2c), to a two-site model. The simulation considered the responses of the apparent two-site parameters both to the increase in the conformational exchange rate constant $k_{ex} = k_1 + k_2$, while $k_1 = k_2$, and to the relative contributions of dissociation-competent and incompetent populations, while the total bound population $p_{b1} + p_{b2}$ remains constant. True values of k_{off}, relaxation, and spectral parameters used to generate the data are listed in the legend of Figure 6.

the apparent values of p_b and R_{2b} may be the consequence of the boundary condition at the fast pulsing limit, which includes the product of these two values (eq 4a). The same trend also exists for the extracted two-site parameters when the relative contribution of the dissociation-competent population was decreased while keeping constant the total bound population $p_b = p_{b1} + p_{b2}$ and the rate k_{ex} of the conformational exchange (Table 3).

Temperature Dependence of the Dissociation Rate Constants Determined by a Two-Site Analysis. The peptide ^{15}N relaxation dispersion profiles were also collected at three different temperatures for the *N*-acetyl-Hir(55−65) peptide in complex with human prothrombin (Table 4 and Figure 7), with an approximate prothrombin/peptide ratio of ∼1:30. The off-rates were calculated for each residue using a two-state model. The two-site k_{off} values of residues Phe$_{56}$, Glu$_{58}$, and Ile$_{59}$ all grow monotonically with temperature and are consistent with one another within the experimental error. Fitting of the temperature dependence of the k_{off} values for these three residues

Table 4. Kinetic and ^{15}N Relaxation Dispersion Parameters of the *N*-Acetyl-Hir(55−65) Peptide in Complex with Human Prothrombin for a Two-Site Exchange Scheme at Different Temperatures (Protein/Peptide Ratio ≈ 1:30)[a]

residue/T	T, K	k_{off}, s^{-1}	$\delta\omega_{bf}$, ppm	p_b, %	R_{2b} [R_{2b}(800)], s^{-1}
Phe56	298	2150 ± 100	−4.2 ± 0.2	2.53 ± 0.15	190 ± 7 [303 ± 18]
Phe56	288	1280 ± 50	−3.4 ± 0.1	4.18 ± 0.15	150 ± 5 [226 ± 9]
Phe56	278	930 ± 40	−3.1 ± 0.1	4.92 ± 0.17	171 ± 5 [257 ± 8]
Glu57	298	2030 ± 200	3.5 ± 0.4	1.92 ± 0.21	400 ± 40 [513 ± 58]
Glu57	288	1200 ± 90	1.9 ± 0.2	5.02 ± 0.21	194 ± 26 [238 ± 34]
Glu57	278	500 ± 50	1.5 ± 0.1	7.18 ± 0.45	201 ± 13 [259 ± 19]
Glu58	298	2210 ± 90	4.3 ± 0.3	4.86 ± 0.39	160 ± 7 [248 ± 17]
Glu58	288	1450 ± 50	4.1 ± 0.2	5.49 ± 0.22	147 ± 4 [254 ± 11]
Glu58	278	1110 ± 50	4.2 ± 0.1	5.27 ± 0.19	204 ± 5 [282 ± 8]
Ile59	298	2260 ± 100	−4.5 ± 0.2	4.41 ± 0.28	193 ± 8 [312 ± 18]
Ile59	288	1170 ± 50	−4.0 ± 0.1	6.01 ± 0.20	189 ± 5 [280 ± 10]
Ile59	278	1020 ± 50	−3.6 ± 0.1	5.86 ± 0.22	260 ± 9 [345 ± 12]

[a] Integration windows of 6(F2) × 16(F1) points at 500 MHz and 4(F2) × 12(F1) points at 800 MHz were used for residue Glu$_{58}$ to increase the accuracy of quantitation for very broad HSQC peaks (see Figure 3).

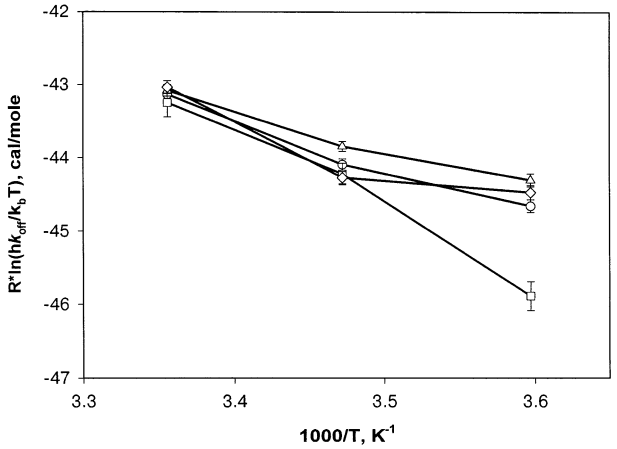

Figure 7. Eyring plots for residues Phe$_{56}$ (○), Glu$_{57}$ (□), Glu$_{58}$ (△), and Ile$_{59}$ (◇). Off-rate constants were calculated using a two-site model (details in Table 4). The plots for residues Phe$_{56}$, Glu$_{58}$, and Ile$_{59}$ estimate the enthalpy of activation ($\Delta H^{\ddagger}$) as 5.8 ± 0.8 kcal/mol and the entropy of activation ($\Delta S^{\ddagger}$) as −24 ± 3 cal/mol K.

to the Eyring equation (Figure 7) yielded estimates of the enthalpy ($\Delta H^{\ddagger}$) and entropy ($\Delta S^{\ddagger}$) of activation as 5.8 ± 0.8 kcal/mol and −24 ± 3 cal/mol K, respectively, for the dissociation of the transient prothrombin−peptide complex. The apparent two-site dissociation rate for residue Glu$_{57}$ appears to be inconsistent with other sites at the lowest temperature used, that is, 5 °C. The apparent intrinsic relaxation and spectral parameters of this residue also had larger variations with the temperature than those for the other three residues (Table 4). These temperature dependence data are again in agreement with the foregoing analysis, pointing to the existence of additional bound conformations for residue Glu$_{57}$ within the transient complex between the *N*-acetyl-Hir(55−65) peptide and human prothrombin.

Discussion

The prothrombin−peptide system is representative of many protein−ligand interactions, whereby the fast dissociation of the complex leads to decreased binding affinities and reduced functional activities of the ligand molecules. In addition, these transient protein−ligand complexes may sample alternative conformations in solution, making the binding energetics rather convoluted and difficult to deal with. Experimental means of quantitating fast dissociation kinetics would therefore be very

valuable for a better understanding of the complex molecular events in transient protein−ligand interactions. We followed the changes in ^{15}N transverse relaxation dispersion of the selectively labeled *N*-acetyl-Hir(55−65) peptide ligand, as a function of the concentration of the binding protein, human prothrombin. We are interested in how well a simple two-site binding model ("bound state-free state") describes the NMR relaxation behavior of the peptide and whether the dissociation rate (k_{off}) can be extracted from ^{15}N NMR relaxation dispersion experiments. Our results show that fast dissociation of protein−peptide complexes can be studied quantitatively by a comparative analysis of the peptide ^{15}N NMR relaxation dispersion profiles of a number of ^{15}N nuclei at two static magnetic fields. The experimental data analysis does not require precise peptide and protein concentrations as long as the binding process can be described by a simple two-site exchange. The ability to follow the relaxation dispersion profiles for every ^{15}N nucleus makes it possible to identify the obviously inconsistent relaxation and kinetic parameters of some residues, which may serve as indicators for the existence of additional conformational exchange processes. Very importantly, the protein titration experiments were shown to improve the accuracy of the dissociation rate constants and other extracted parameters and, under certain conditions, make it possible to quantitate the rate of conformational changes within the protein−peptide complex.

For the binding of the 11-residue antithrombin peptide with human prothrombin, every one of the five ^{15}N labeled adjacent residues of the peptide displayed slightly different relaxation and exchange behaviors. Transverse relaxation of residue Asp_{55} showed a very weak response to the complex formation, implying a small change in chemical shift upon binding. This is in accordance with the weak response of the binding affinity of recombinant hirudin to the Asp_{55}Asn amino acid substitution[65] and of the hirudin peptide to the Asp_{55}Gly replacement.[66] Residues Phe_{56} and Ile_{59} had significantly increased transverse relaxation in the presence of prothrombin and followed a two-site exchange model fairly well, independent of the prothrombin concentration. Both of these residues were shown to be important for binding of all hirudin-based peptides and involved in extensive hydrophobic interactions with thrombin.[66−68] One can estimate the K_D for the interaction of the *N*-acetyl-Hir(55−65) peptide with human prothrombin to be approximately 100−300 μM.[44,45] If one assumes the k_{on} for *N*-acetyl-Hir(55−65) to be in the range of 10^7−10^8 M^{-1} s^{-1}, as reported for hirudin-based peptides,[65,69,70] we can calculate $k_{off} = K_D k_{on}$ as 10^3−10^4 s^{-1}, in good agreement with the k_{off} value determined here by use of ^{15}N NMR relaxation dispersion spectroscopy (Tables 1 and 2). In addition, the transient prothrombin−peptide complex appears to have a rather low enthalpy of activation ($\Delta H^{\dagger} \approx 6$ kcal/mol) and a much more negative entropy of activation ($-\Delta S^{\dagger} \approx 24$ cal/mol K) for dissociation in comparison to some high-affinity protein−ligand complexes.[10] Interestingly, the binding surface of prothrombin for the peptide was shown to engage in primarily hydrophobic interactions with a protein inhibitor, with the binding driven mostly by entropic contributions.[71]

A residue Glu_{57} of the peptide displayed a relaxation behavior suggesting the presence of alternatively bound states in complex with prothrombin. Although the relaxation dispersion curves of Glu_{57} could be fitted to a two-state exchange model, the apparent transverse relaxation rates (R_{2b}) for Glu_{57} in the complex were significantly higher, whereas the fraction of the peptide in the bound state (p_b) was lower than those determined for Phe_{56} and Ile_{59}. We established that more realistic values of R_{2b} and p_b can be obtained by extending the exchange model to a three-state process and by the analysis of the peptide ^{15}N relaxation data at all three prothrombin concentrations simultaneously. The "linear" three-state model (Figure 2C) deduced for Glu_{57} is a natural consequence of the kinetic data obtained by stopped-flow fluorescence spectroscopy.[72] Jackman et al. demonstrated that the binding of a hirudin peptide Hir(52−65) with thrombin can be interpreted in terms of the same two-step kinetic mechanism (Figure 2C). Although in the stopped-flow experiments, the intrinsic fluorescence of thrombin was used to detect formation of the intermediates, it is feasible that the peptide would respond synchronously to the conformational changes in the binding protein. It appears that both prothrombin and thrombin may undergo similar conformational exchanges upon binding of the peptide. In fact, the fitted k_1 and k_2 rates for the conformational change were on the order of $\sim 10^2$ s^{-1} for the prothrombin−peptide complex which is comparable with those ($\sim$115 and $\sim$185 s^{-1}, respectively) obtained for thrombin−peptide interactions.[72] We also showed that the k_{off} value obtained from the "linear" three-site exchange scheme is underestimated by a two-site model fitting but not dramatically. For a site with alternative binding modes, the population-averaged k_{off}^{app} rate constant is close to the k_{off} value obtained for other residues (i.e., Phe_{56} and Ile_{59}), obeying two-site exchange.

To summarize, binding of the antithrombin peptide to prothrombin appears to involve complex kinetic processes, with some sites of the peptide showing predominantly a two-state behavior, while other sites can sense additional bound states. These kinetic processes can be studied quantitatively through peptide NMR relaxation dispersion experiments at a number of concentrations of the binding protein. The ability to dissect at atomic resolution the kinetic events of weak and specific binding of peptide ligands with large proteins, such as prothrombin, offers exciting opportunities for probing ligand interactions with pharmaceutically interesting but ill-characterized protein targets.

Acknowledgment. This work was inspired by a number of stimulating discussions with Prof. J. Feeney of MRC, Mill Hill, England. We thank Dr. Michael Osborne for helpful comments. We are also grateful to the reviewers for the many insightful and constructive criticisms and suggestions. This work was supported in part by the Genomics and Health Initiative of the Government of Canada and by the National Research Council of Canada (NRCC Publication No. 46159).

JA021238L

(65) Betz, A.; Hofsteenge, J.; Stone, S. R. *Biochem. J.* **1991**, *275* (Pt 3), 801−803.
(66) Yue, S. Y.; DiMaio, J.; Szewczuk, Z.; Purisima, E. O.; Ni, F.; Konishi, Y. *Protein Eng.* **1992**, *5*, 77−85.
(67) Skrzypczak-Jankun, E.; Carperos, V. E.; Ravichandran, K. G.; Tulinsky, A.; Westbrook, M.; Maraganore, J. M. *J. Mol. Biol.* **1991**, *221*, 1379−1393.
(68) Qiu, X.; Padmanabhan, K. P.; Carperos, V. E.; Tulinsky, A.; Kline, T.; Maraganore, J. M.; Fenton, J. W. *Biochemistry* **1992**, *31*, 11689−11697.
(69) Skordalakes, E.; Elgendy, S.; Goodwin, C. A.; Green, D.; Scully, M. F.; Kakkar, V. V.; Freyssinet, J. M.; Dodson, G.; Deadman, J. J. *Biochemistry* **1998**, *37*, 14420−14427.
(70) Myles, T.; Le Bonniec, B. F.; Betz, A.; Stone, S. R. *Biochemistry* **2001**, *40*, 4972−4979.
(71) Monteiro, R. Q.; Bock, P. E.; Bianconi, M. L.; Zingali, R. B. *Protein Sci.* **2001**, *10*, 1897−1904.
(72) Jackman, M. P.; Parry, M. A.; Hofsteenge, J.; Stone, S. R. *J. Biol. Chem.* **1992**, *267*, 15375−15383.